RSC Advances

PAPER

View Article Online
View Journal | View Issue

Cite this: *RSC Adv.*, 2017, **7**, 32310

Pd–Ni nanoparticles supported on reduced graphene oxides as catalysts for hydrogen generation from hydrazine†

Ya Chen,[a] Ling Wang,[b] Yanan Zhai,[b] Heyin Chen,[b] Yibo Dou,[a] Jianrong Li,*[a] Haoquan Zheng*[b] and Rui Cao*[ab]

Received 19th April 2017
Accepted 19th June 2017

DOI: 10.1039/c7ra04390b

rsc.li/rsc-advances

A composite material of Pd–Ni nanoparticles supported on reduced graphene oxide (Pd–Ni/rGO) has been synthesised *via* an *in situ* reduction of PdO/$Ni(OH)_2$ nanoparticles on GO. This Pd–Ni/rGO material is characterised by powder X-ray diffraction, transmission electron microscopy, scanning electron microscopy and X-ray photoelectron spectroscopy. The molar ratio of Pd/Ni in the alloy nanoparticles can be fine tuned by changing the starting ratio of Pd/Ni precursors during synthesis. The bimetallic Pd_3Ni/rGO exhibits high catalytic activity, selectivity, and durability toward the hydrogen generation from hydrazine, while corresponding monometallic (Pd/rGO or Ni/rGO) counterparts are either inactive or poorly active under analogous reaction conditions.

1. Introduction

Hydrogen is a globally accepted clean fuel due to its high efficiency and power density.[1–3] High hydrogen content (8.0 wt%) and easy recharging make hydrazine a promising hydrogen carrier.[4–6] Furthermore, hydrazine is a liquid-phase material, which has the potential to take the advantage of the existing liquid-based distribution infrastructure. Transition metals are usually considered as the ideal candidates for hydrogen generation from hydrazine.[7–13] However, monometallic catalysts are either inactive or poorly active in this reaction.[4,14,15] In comparison, bimetallic materials, especially Ni-based bimetallic materials, are of great importance for the electrochemical production of hydrogen from hydrazine due to the synergetic effect from the inter-metallic combinations of different metals.[16–28] These bimetallic systems exhibit fast reaction kinetics and high selectivity toward hydrogen generation.

Ultra-small metal nanocatalysts (<7 nm) have received substantial attention, because they show high catalytic efficiencies in numerous reactions.[29–33] However, the broad particle size distribution and the aggregation of metal NPs during reaction limit their applications. Supports can be used to solve this problem.[34] Among all the supports, the reduced graphene oxide (rGO) is an ideal one because of its large surface area, good electrical conductivity, and excellent mechanical strength.[35–37]

Metal NPs/rGO composite materials have been synthesised and used as nanocatalysts. Impregnation and coprecipitation are current manufacturing methods to introduce metal NPs on rGO, where metal salts were first adsorbed on rGO and then reduced by $NaBH_4$. The obtained metal NPs have a broad size distribution from a few nanometers to micrometers. Although the use of surfactant can narrow the size distribution, the catalytic activity decreases unfortunately.[38–40] Recently, an *in situ* reduction approach has been developed.[41–43] Instead of loading metal ions on rGO, metal oxide NPs with a narrow particle size distribution were loaded onto graphene oxide (GO). Metal oxide NPs and GO were then reduced to metal NPs and rGO, respectively, by $NaBH_4$ in one pot. Here, we synthesise a composite material of Pd–Ni bimetallic NPs supported on reduced graphene oxide (Pd–Ni/rGO) *via* an *in situ* reduction of PdO/$Ni(OH)_2$ NPs on GO. This novel catalytic system was found to display efficient activity and high selectivity for dehydrogenation of alkaline solution of hydrazine.

[a]*Beijing Key Laboratory for Green Catalysis and Separation, Department of Chemistry and Chemical Engineering, College of Environmental and Energy Engineering, Beijing University of Technology, Beijing 100124, P. R. China. E-mail: ruicao@ruc.edu.cn; jrli@bjut.edu.cn*

[b]*Key Laboratory of Applied Surface and Colloid Chemistry, Ministry of Education, School of Chemistry and Chemical Engineering, Shaanxi Normal University, Xi'an 710119, China. E-mail: zhenghaoquan@snnu.edu.cn*

† Electronic supplementary information (ESI) available: XRD patterns and EDX of Pd_3Ni/rGO, photographs of Na_2PdCl_4, $PdO \cdot H_2O$, $NiCl_2$ and $Ni(OH)_2$ and durability test of Pd_3Ni/rGO after different cycles. See DOI: 10.1039/c7ra04390b

2. Experimental section

2.1 Chemicals

Graphene oxide (GO) was purchased from Nanjing XFNANO Materials TECH Co., Ltd. The following reagents were purchased from Sinopharm Chemical Reagent Co., Ltd. and used without purification: $PdCl_2$, $NiCl_2$, $NaBH_4$, and NaOH.

2.2 Synthesis of materials

Synthesis of the Pd/rGO composites and Ni/rGO composites. In a typical procedure, 1.21 mL of 0.1 M H_2PdCl_4 solution was added into an as-prepared 10 mL 3 mg mL^{-1} of GO suspension and stirred for 10 min. After adjusting the pH of the mixture to 6.5, the suspension was heated at 40 °C for 6 h. Then, 6 mL 1 M $NaBH_4$ of solution was added into the suspension and stirred for 60 min. After the reaction, the obtained Pd/rGO composites were separated by centrifugation at 6000 rpm, and then dried at 50 °C for 12 h in a vacuum dryer.

The same process was used as that used for the Ni/rGO composites, with the 1.21 mL of 0.1 M H_2PdCl_4 solution replaced by 2.18 mL of 0.1 M $NiCl_2$ solution.

Synthesis of the Pd_3Ni/rGO composites. In a typical procedure, 1.023 mL of 0.1 M H_2PdCl_4 and 0.341 mL of 0.1 M $NiCl_2$ solution was added into an as-prepared 10 mL 3 mg mL^{-1} of GO suspension and stirred for 10 min. After adjusting the pH of the mixture to 8, the suspension was heated at 40 °C for 6 h. A solution of 7 mL 1 M $NaBH_4$ was added into the suspension and stirred for 60 min. After the reaction, the obtained Pd_3Ni/rGO composites were separated by centrifugation at 6000 rpm, and then dried at 50 °C for 12 h in a vacuum dryer. The preparation of the PdNi/rGO and $PdNi_3$/rGO is following the analogous process. For PdNi/rGO composites, 0.78 mL of 0.1 M H_2PdCl_4, 0.78 mL of 0.1 M $NiCl_2$ and 8 mL 1 M $NaBH_4$ were used, while 0.454 mL of 0.1 M H_2PdCl_4, 1.362 mL of 0.1 M $NiCl_2$ and 9 mL 1 M $NaBH_4$ were used to synthesise $PdNi_3$/rGO.

2.3 Catalytic activities

Catalytic reactions were carried out using a two-necked round bottom flask which contained the as prepared nanocatalysts (20 mg). One neck of the flask was connected to a gas burette and the other was connected to a pressure-equalization funnel to introduce 18 mL NaOH (0.5 M). The suspension was stirred for 30 min, and then 2 mL of solution containing $N_2H_4 \cdot H_2O$ (0.5 M) was added. The catalytic reaction was begun once the hydrazine aqueous solution was added into the catalyst suspension in the flask with magnetic stirring at 323 K. The evolution of gas was monitored using the gas burette. The selectivity toward H_2 generation can be calculated using equation: $X = (3\lambda - 1)/8$ [$\lambda = n(H_2 + N_2)/n(H_2NNH_2)$].

The reactions over Pd_3Ni/rGO composites were carried out at different temperatures (303, 313, 323, 333 and 343 K) to evaluate their activation energies for the decomposition of hydrazine in aqueous solution under ambient atmosphere.

3. Results and discussions

As shown in Fig. 1, GO that has –OH and –COOH groups without any further functionalisation was directly purchased and used as supports. A stock solution of H_2PdCl_4 and $NiCl_2$ was prepared. Then, the stock solution and GO were mixed. The pH of the solution was adjusted to 8 by NaOH, so that PdO/$Ni(OH)_2$ nanoparticles were loaded onto GO due to the strong interaction between them and functional groups on GO. The suspension was then reduced by $NaBH_4$. The molar ratios of Pd and Ni in Pd–Ni/rGO hybrid materials can be tuned by changing the $H_2PdCl_4/NiCl_2$ ratio in the stock solutions. The bimetallic systems were denoted as Pd_3Ni/rGO, PdNi/rGO and $PdNi_3$/rGO with the Pd : Ni molar ratio of 3 : 1, 1 : 1 and 1 : 3, respectively. The monometallic systems were denoted as Pd/rGO and Ni/rGO, respectively.

Fig. 2 shows the powder X-ray diffraction (PXRD) patterns of Pd–Ni/rGO hybrid materials. There is no diffraction peak at 10.3°, corresponding to the (001) reflection of graphene oxide, which demonstrates the full reduction of GO. The diffraction peaks of Pd/rGO at 40.1, 46.1, 67.4, and 81.5° correspond to (111), (200), (220) and (311) facets of face centred cubic (fcc) crystal structured Pd NPs (Fig. 2, red bar, JCPDS 5-681), while

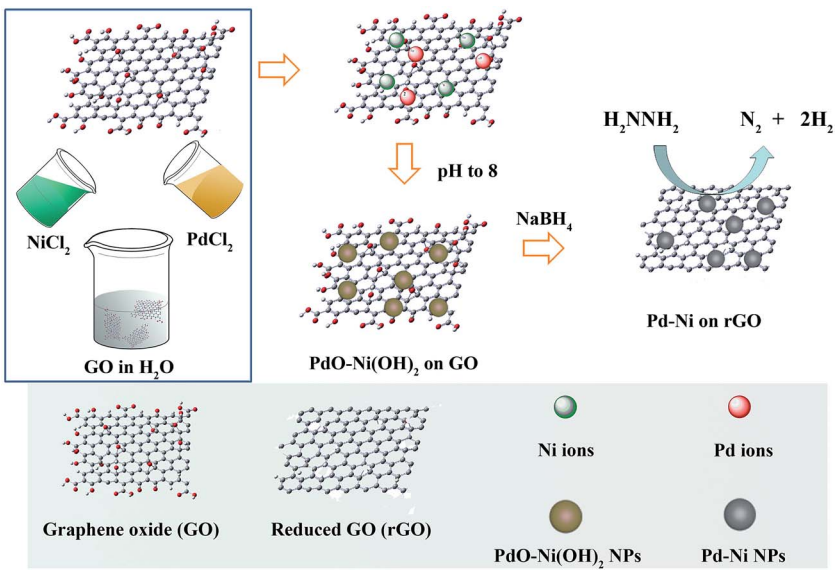

Fig. 1 Schematic illustration for the synthesis of Pd–Ni/rGO catalysts.

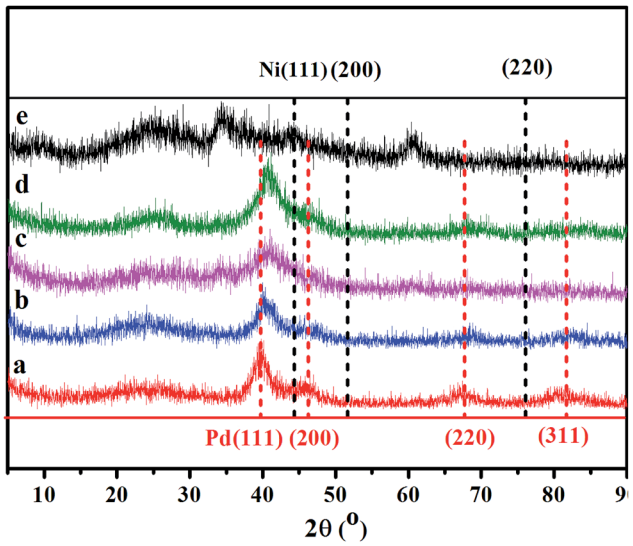

Fig. 2 PXRD patterns of Pd/rGO (a), Pd_3Ni/rGO (b), PdNi/rGO (c), $PdNi_3$/rGO (d) and Ni/rGO (e).

the peaks of Ni/rGO at 44.8, 52.0 and 76.6° are assigned to the (111), (200), and (220) facets of Ni NPs. For Ni/rGO, the peaks of NiO can also be observed. Compared with the monometallic systems, no individual peak of pure Ni or Pd NPs was observed in the PXRD profiles of Pd–Ni/rGO. The representative diffraction peaks of Pd–Ni/rGO are coincidently located between peaks of Pd/rGO and those of Ni/rGO (Fig. 2), demonstrating that the partial Ni has entered into the Pd lattice and an alloy of Pd–Ni was formed. The crystal size of Pd–Ni/rGO is estimated to be 5 nm according to the Scherrer formula.[44]

The adjustment of pH by a solution of NaOH before reduction is important for the formation of Pd–Ni alloy NPs. In principle, Pd and Ni are miscible and can form alloy all over the phase diagram with fcc structures.[45] However, if the pH was not adjusted, the PXRD pattern of the Pd–Ni/rGO is a combined crystalline feature of Pd and Ni, indicating the coexistence of these components (Fig. S1†).

The morphology and surface structure of Pd_3Ni/rGO, that shows the highest activity in hydrogen generation from hydrazine (see results in catalytic reaction), were further investigated by scanning electron microscopy (SEM), transmission electron microscopy (TEM) and X-ray photoelectron spectroscopy (XPS) (Fig. 3). The TEM image shows a 2D nanosheet, which is the typical morphology of rGO (Fig. 3a). No big particle on nanosheet was observed, suggesting the homogenous distribution of Pd_3Ni NPs on the rGO. Fig. 3b shows the SEM image and the energy-dispersive X-ray spectroscopy (EDS) mapping of the same area. Both Pd and Ni elements were distributed in a well-dispersed pattern throughout the whole area. The atomic ratio of Pd/Ni is 2.71, which is consistent with the expected composition of Pd_3Ni (Fig. S2†). The XPS of Pd_3Ni/rGO exhibits characteristic signals for Pd^0 and Ni^0, indicating the coexistence of both metals (Fig. 3c and d).[9] The binding energies in the Pd[$3d_{5/2}$] for the bimetallic Pd_3Ni/rGO nanocatalysts shifted to higher value demonstrating the alloy formation.[16] The percentage of Pd^0 and Ni^0 species in Pd_3Ni/rGO composites is calculated to be 82.35 and 76.21%, respectively. The oxidized Pd and Ni species in XPS may be formed during the sample preparation.

The spherical Pd_3Ni NPs are well-dispersed on the rGO (Fig. 4a). The size distribution of Pd_3Ni NPs on the rGO surface was measured from TEM images, showing a high uniformity

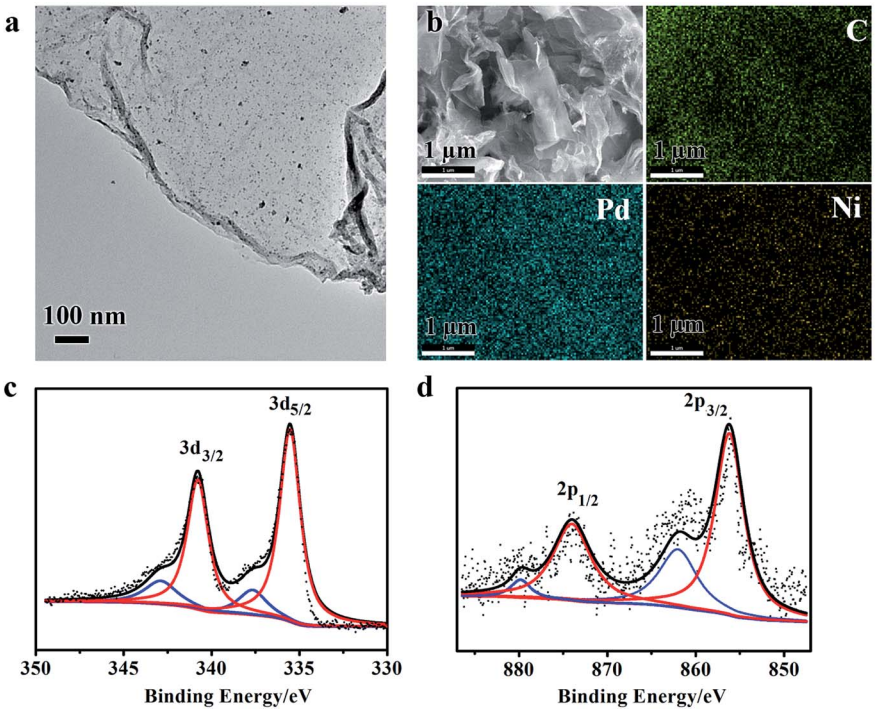

Fig. 3 TEM image (a), SEM image and corresponding EDS mapping (b), and XPS spectra (c and d) of Pd and Ni of Pd_3Ni/rGO catalyst, respectively.

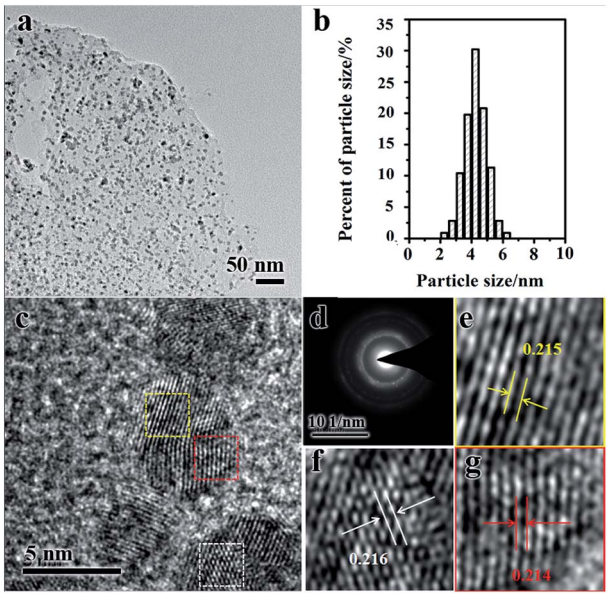

Fig. 4 TEM image (a), the average diameter and distribution (b), high resolution TEM image (c) and SAED (d) of Pd_3Ni/rGO catalyst. (e, f and g) Enlarged image of three areas in (c).

with an average diameter of 4.3 and a standard deviation of *ca.* 16% (Fig. 4b). The metal NPs in metal NPs/rGO composites have similar particle sizes as the original metal oxide NPs have (Fig. S3†). High resolution TEM (HRTEM) image shows well-resolved lattice fringes in Pd_3Ni NPs (Fig. 4c). The selected area electron diffraction (SAED) of Pd_3Ni NPs on rGO gives a ring-like pattern (Fig. 4d), which suggests a random orientation of the Pd_3Ni nanocrystals. The clear lattice fringes with an average value of 0.214 nm can demonstrate the crystalline nature of fcc Pd_3Ni alloy, which is between the Pd (111) crystal plane (0.224 nm) and the Ni (111) plane (0.203 nm) (Fig. 4e–g). The loading of Pd_3Ni is 34.19 wt%. It is worth emphasizing that the control of particle size of metal NPs with high loading (>30 wt%) is quite challenging. High loadings of metal NPs may induce the aggregation of NPs. In this work, the hybrid metal oxide NPs of $PdO/Ni(OH)_2$ on GO were synthesised as precursors. The particle size of metal oxides was easy to control. Then, the *in situ* reduction approach were used. The particle size of NPs on GO does not change during the reduction. The *in situ* reduction approach shows advantages in the control of particle size compared to the post-reduction procedure.

To investigate the dependence of activity and hydrogen selectivity on the Pd/Ni ratio, the Pd–Ni/rGO materials have been tested for the catalytic dehydrogenation of aqueous solution of hydrazine at 50 °C in the presence of 0.5 M NaOH (Fig. 5a). For all Pd–Ni/rGO nanocatalysts, an initiation release of gas can be observed as soon as the hydrazine was added. The amount of resulting gas was used to evaluate the selectivity towards hydrogen in this reaction. The activities of the catalysts were strongly dependent on the composition of Pd–Ni NPs,

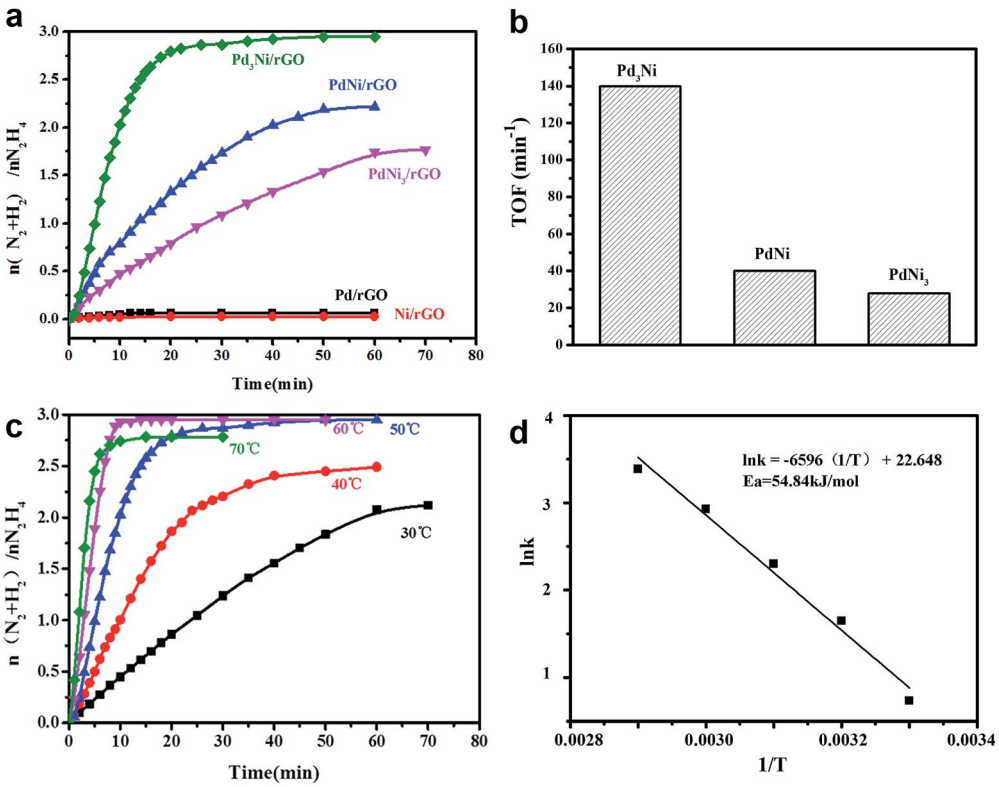

Fig. 5 (a) Time course plots for the decomposition of aqueous solution of hydrazine over Pd–Ni/rGO with NaOH (0.5 M) at 50 °C (catalyst = 0.02 g; $N_2H_4 \cdot H_2O$ = 2 mL). (b) TOF of Pd_3Ni/rGO, PdNi/rGO and $PdNi_3$/rGO. (c) Time course plots for hydrogen generation by the decomposition of hydrazine by Pd_3Ni/rGO at 30, 40, 50, 60 and 70 °C. (d) The plot of ln *k* *vs.* 1/*T*.

while monometallic systems, for both Pd/rGO and Ni/rGO, show poor catalytic activities (less than 0.2 equiv. of gas was release). When Pd was alloyed to Ni, the bimetallic system of $PdNi_3$/rGO exhibits the activity for the dehydrogenation of hydrazine with the hydrogen selectivity of 54.2% and the turnover frequency (TOF) value of 27.88 min^{-1} at 50 °C (Fig. 5b). The catalytic activity of $PdNi_3$/rGO is poor (1.5 equiv. of gas was released over 3 h). A higher hydrogen selectivity of 70.7% and a higher catalytic activity with the TOF value of 40.05 min^{-1} were observed, when the Pd : Ni ratio further increased to 1 : 1. Among all catalysts, Pd_3Ni/rGO exhibits the highest catalytic activity with TOF value of 140 min^{-1} and 100% hydrogen selectivity, which shows better selectivity than previously reported work.[16] In order to obtain the activation energy (E_a) of the dehydrogenation of hydrazine catalysed by Pd_3Ni/rGO, the catalytic experiments were carried out at temperatures ranging from 30 to 70 °C (Fig. 5c and d). The E_a was calculated based on following equation: $E_a = RT \ln A/k$, where k is chemical reaction rate, T is temperature in kelvin, A is pre-exponential factor and R is gas constant. The E_a was determined to be 54.84 kJ mol^{-1}, which is close to the reported values.[6,16] The as-synthesised Pd_3Ni/rGO was tested in terms of durability in three cyclic usages (Fig. S4†). The loss of activities might be caused by leaching of nanocatalysts, where the loading decrease to 28.3% after three cycles. The functionalization of rGO with function groups may improve the stability of the catalysts.

The existence of Ni and Pd metals in an alloy state is a key factor behind the observed high catalytic performance.[46] The monometallic Pd/rGO and Ni/rGO nanocatalysts show poor catalytic activity for the hydrogen generation from hydrazine, while the presence of both metals with inter-metallic Ni–Pd bonding on the catalyst active centres is vital for the activation of bonds in hydrazine for hydrogen generation. The rGO supports are also important, because they prevent the aggregation of Pd_3Ni NPs during the dehydrogenation.

4. Conclusions

We have developed a composite material of Pd–Ni/rGO as an efficient heterogeneous catalyst for dehydrogenation of hydrazine. The well-dispersed Pd–Ni NPs on rGO have been successfully prepared by an *in situ* reduction of $PdO/Ni(OH)_2$ on GO, which prevents the further aggregation of Pd–Ni NPs during the reduction process. Bimetallic systems (Pd–Ni/rGO) exhibit the high catalytic activity toward dehydrogenation of hydrazine, while the pure metal systems (Pd/rGO and Ni/rGO) show no generation of hydrogen from hydrazine. Among them, Pd_3Ni/rGO catalyst shows highest catalytic activity and exhibits 100% hydrogen selectivity. The high activity and selectivity enables Pd_3Ni/rGO material as a potential catalyst for practical applications in dehydrogenation of alkaline solution of hydrazine for hydrogen storage in the future.

Acknowledgements

We thank the financial support from the "Thousand Talents Program" of China, the National Natural Science Foundation of China (No. 21576006, 21101170, 21573139 and 21601118). We thank Prof. Yu Chen for valuable discussions and comments.

Notes and references

1 H. B. Gray, *Nat. Chem.*, 2009, **1**, 7.
2 C. G. Morales-Guio, L.-A. Stern and X. Hu, *Chem. Soc. Rev.*, 2014, **43**, 6555–6569.
3 X. Zou and Y. Zhang, *Chem. Soc. Rev.*, 2015, **44**, 5148–5180.
4 S. K. Singh, X.-B. Zhang and Q. Xu, *J. Am. Chem. Soc.*, 2009, **131**, 9894–9895.
5 M. Yadav and Q. Xu, *Energy Environ. Sci.*, 2012, **5**, 9698–9725.
6 N. Cao, L. Yang, H. Dai, T. Liu, J. Su, X. Wu, W. Luo and G. Cheng, *Inorg. Chem.*, 2014, **53**, 10122–10128.
7 S. K. Singh and Q. Xu, *J. Am. Chem. Soc.*, 2009, **131**, 18032–18033.
8 S. K. Singh, A. K. Singh, K. Aranishi and Q. Xu, *J. Am. Chem. Soc.*, 2011, **133**, 19638–19641.
9 L. He, Y. Huang, A. Wang, X. Wang, X. Chen, J. J. Delgado and T. Zhang, *Angew. Chem., Int. Ed.*, 2012, **51**, 6191–6194.
10 T. He, H. Wu, G. Wu, J. Wang, W. Zhou, Z. Xiong, J. Chen, T. Zhang and P. Chen, *Energy Environ. Sci.*, 2012, **5**, 5686–5689.
11 Z. Huang and T. Autrey, *Energy Environ. Sci.*, 2012, **5**, 9257–9268.
12 J. Wang, X.-B. Zhang, Z.-L. Wang, L.-M. Wang and Y. Zhang, *Energy Environ. Sci.*, 2012, **5**, 6885–6888.
13 L. He, Y. Huang, A. Wang, X. Wang and T. Zhang, *AIChE J.*, 2013, **59**, 4297–4302.
14 S. K. Singh and Q. Xu, *Chem. Commun.*, 2010, **46**, 6545–6547.
15 S. K. Singh and Q. Xu, *Inorg. Chem.*, 2010, **49**, 6148–6152.
16 S. K. Singh, Y. Iizuka and Q. Xu, *Int. J. Hydrogen Energy*, 2011, **36**, 11794–11801.
17 H.-L. Wang, J.-M. Yan, S.-J. Li, X.-W. Zhang and Q. Jiang, *J. Mater. Chem. A*, 2015, **3**, 121–124.
18 Y.-J. Zhong, H.-B. Dai, Y.-Y. Jiang, D.-M. Chen, M. Zhu, L.-X. Sun and P. Wang, *J. Power Sources*, 2015, **300**, 294–300.
19 C. Li, T. Wang, W. Chu, P. Wu and D. G. Tong, *Nanoscale*, 2016, **8**, 7043–7055.
20 G. Yao, F. Chen, Z. Huo and F. Jin, *Int. J. Hydrogen Energy*, 2016, **41**, 9135–9139.
21 X. Miao, M. M. Chen, W. Chu, P. Wu and D. G. Tong, *ACS Appl. Mater. Interfaces*, 2016, **8**, 25268–25278.
22 S. De, J. Zhang, R. Luque and N. Yan, *Energy Environ. Sci.*, 2016, **9**, 3314–3347.
23 J. Chen, Q. Yao, J. Zhu, X. Chen and Z.-H. Lu, *Int. J. Hydrogen Energy*, 2016, **41**, 3946–3954.
24 Z. Zhang, Z.-H. Lu and X. Chen, *ACS Sustainable Chem. Eng.*, 2015, **3**, 1255–1261.
25 Z. Zhang, Z.-H. Lu, H. Tan, X. Chen and Q. Yao, *J. Mater. Chem. A*, 2015, **3**, 23520–23529.
26 Y. Zhao, X. Yang, J. Tian, F. Wang and L. Zhan, *Int. J. Hydrogen Energy*, 2010, **35**, 3249–3257.
27 W. Gao, C. Li, H. Chen, M. Wu, S. He, M. Wei, D. G. Evans and X. Duan, *Green Chem.*, 2014, **16**, 1560–1568.
28 D. Bhattacharjee, K. Mandal and S. Dasgupta, *J. Power Sources*, 2015, **287**, 96–99.

29 B. Liu, H. Yao, W. Song, L. Jin, I. M. Mosa, J. F. Rusling, S. L. Suib and J. He, *J. Am. Chem. Soc.*, 2016, **138**, 4718–4721.
30 L. Bai, X. Wang, Q. Chen, Y. Ye, H. Zheng, J. Guo, Y. Yin and C. Gao, *Angew. Chem.*, 2016, **128**, 15885–15890.
31 T. Imaoka, H. Kitazawa, W.-J. Chun and K. Yamamoto, *Angew. Chem., Int. Ed.*, 2015, **54**, 9810–9815.
32 H. Wei, X. Liu, A. Wang, L. Zhang, B. Qiao, X. Yang, Y. Huang, S. Miao, J. Liu and T. Zhang, *Nat. Commun.*, 2014, **5**, 5634.
33 A. Corma, P. Concepción, M. Boronat, M. J. Sabater, J. Navas, M. J. Yacaman, E. Larios, A. Posadas, M. A. López-Quintela, D. Buceta, E. Mendoza, G. Guilera and A. Mayoral, *Nat. Chem.*, 2013, **5**, 775–781.
34 J. Li, P. Zhou, F. Li, R. Ren, Y. Liu, J. Niu, J. Ma, X. Zhang, M. Tian, J. Jin and J. Ma, *J. Mater. Chem. A*, 2015, **3**, 11261–11268.
35 J. Shi, Q. Ji, Z. Liu and Y. Zhang, *Adv. Energy Mater.*, 2016, **6**, DOI: 10.1002/aenm.201600459.
36 Q. Yao, Z.-H. Lu, W. Huang, X. Chen and J. Zhu, *J. Mater. Chem. A*, 2016, **4**, 8579–8583.
37 W.-d. Zhong, X.-k. Tian, C. Yang, Z.-x. Zhou, X.-w. Liu and Y. Li, *Int. J. Hydrogen Energy*, 2016, **41**, 15225–15235.
38 Y. Liu, H. Tsunoyama, T. Akita, S. Xie and T. Tsukuda, *ACS Catal.*, 2011, **1**, 2–6.
39 Z. Niu and Y. Li, *Chem. Mater.*, 2014, **26**, 72–83.
40 M. Cargnello, C. Chen, B. T. Diroll, V. V. T. Doan-Nguyen, R. J. Gorte and C. B. Murray, *J. Am. Chem. Soc.*, 2015, **137**, 6906–6911.
41 L. Fumin, G. Xueqing, X. Qi, L. Shuni, C. Yu and L. Jong-Min, *Nanotechnology*, 2015, **26**, 065603.
42 X. Gao, F. Li, Y. Li, S. Li, Y. Chen and J.-M. Lee, *J. Power Sources*, 2015, **280**, 491–498.
43 X. Gao, Y. Li, Q. Zhang, S. Li, Y. Chen and J.-M. Lee, *J. Mater. Chem. A*, 2015, **3**, 12000–12004.
44 A. L. Patterson, *Phys. Rev.*, 1939, **56**, 978–982.
45 C. Paduani, *J. Magn. Magn. Mater.*, 2011, **323**, 2076–2079.
46 S. N. Oliaee, C. Zhang, S. Y. Hwang, H. M. Cheung and Z. Peng, *J. Phys. Chem. C*, 2016, **120**, 9764–9772.